

Image Compression Using Noise Reduction

Deepti Gaonkar¹, Dr. Rajiv Yadhav²

¹Research Scholar, Department of Computer Science, OPJS University, Churu, Rajasthan

²Research Supervisor, Department of Computer Science, OPJS University, Churu, Rajasthan

Abstract

Noise is present in digitally captured images. Adding more noise to a picture reduces its ability to be recognized. To enhance the precision of picture identification, noise reduction is crucial. An image's noise may be reduced with the use of a low-pass filter, such as a Gaussian filter (GF). Using a low-pass filter may help lessen the volume of background noise. Low-pass filters, however, always have that effect. The reliability of edge and feature identification in picture recognition degrades as blurring of the edges increases. Therefore, we present a GF+L2-norm hybrid noise reduction filter for pictures, which is capable of maintaining sharpness along image edges. By enhancing picture quality, the suggested strategy should also boost the reliability of image recognition.

Keywords: *Soft Morphology, Noise Reduction, Periodic Noise, digital image processing, L2-norm*

1. INTRODUCTION

In image processing, noise comes in many forms. (1) photoelectronic noise, also known as photon noise; (2) impulse noise, which includes phenomena like salt and pepper and line drop; and (3) structured noise, which includes phenomena like periodic and aperiodic noise, detector striping noise, and so on. The frequency domain is often used to analyze periodic noise. The frequency transform aggregates periodic noise in an image into a small number of spikes that may be removed. This noise might originate from the image sensor or from electrical interference. Figure 1 depicts the Lenna picture with periodic noise (sinusoidal noise) superimposed on it. Figure 1 displays the frequency domain noise spikes. Conventionally, a suitably tuned band-reject filter will be employed for decreasing the periodic noise without adversely affecting the picture quality. It is well acknowledged that automatically recognizing noise spikes is challenging. The power spectrum assessment of narrow band noise cannot be readily accomplished. Because of the computational burden, visual identification of noise spikes in the frequency domain is impractical for processing a large number of pictures. It also takes a long time for signals to be converted between the spatial and frequency domains. One of the spatial domain approaches, the soft morphology filter is presented in this letter to dramatically enhance the computing efficiency for periodic noise reduction.

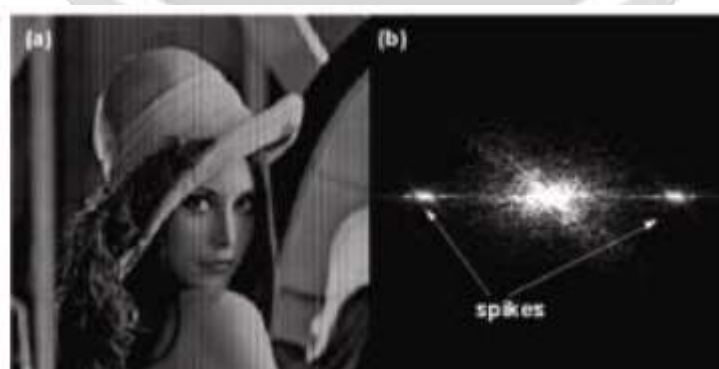


Figure 1. depicts the Lenna picture with periodic noise (sinusoidal noise) superimposed on it

Noise reduction is the process of reducing noise from a signal. Noise reduction methods exist for audio and visuals. Noise reduction methods may distort the signal to some degree. Noise rejection is the ability of a circuit to separate an undesirable signal component from the desired signal component, as with common-mode

rejection ratio. Analog and digital signal processors both are vulnerable to noise because of certain design choices. Noise may be either uniformly distributed in frequency (white noise) or frequency-dependent, introduced by the device's mechanism or signal-processing algorithms. Hiss is a common kind of electronic system noise caused by the chaotic migration of electrons in response to fluctuations in temperature. Noise is produced when these excited electrons quickly add and remove to the output signal.

The grain structure of both photographic film and magnetic tape introduces noise (both apparent and auditory) into the recording. The sensitivity of photographic film is determined by the size of the film's individual grains; more sensitive film will have larger-sized grains. Noise on magnetic tape increases as the magnetic particles (often ferric oxide or magnetite) get greater in size. To compensate for this, bigger regions of film or magnetic tape may be utilized to minimize the noise to a tolerable level.

2. LITERATURE REVIEWS

Catalin Dumitrescu (2020) Mathematically speaking, wavelets are a fascinating topic of study, and practically speaking, they are a helpful tool in many applications, including picture compression, signal/noise enhancement, numerical analysis, and the like, in subjects as diverse as statistics, physics, and geology. There is no one universal technique for processing wavelet coefficients; instead, it varies depending on whether the application is one of data compression, signal analysis, noise reduction, statistical estimation, or detection. Not only that, but the most valuable attributes of wavelet transformation vary from usage to use. To that end, this paper presents a novel filter that uses local statistics based on wavelet transformations to enhance picture quality, as well as a measure for the quantitative assessment of contour retention after processing, and a technique for calculating the noise dispersion in images.

Abdalla Mohamed Hambal (2017) Noises are a common image quality issue. Background noise is something that may be gained or created during the imaging process. In the field of image processing, removing noise is a crucial step. In most cases, the standard of the image processing methods is significantly impacted by the outcomes of the noise reduction. In color image processing, many methods for eliminating noise have been successfully implemented. What kind of noise is interfering with the picture will determine how complex the challenge of removing that noise will be. Many filtering strategies, both linear and nonlinear, have been developed for use in the quest to reduce the amount of noise seen in images. Since linear filters have a propensity to distort the edges of a picture, they are not able to properly remove impulsive noise. However, nonlinear filters excel at suppressing impulsive noise. In recent years, a number of nonlinear filters using both Classical and fuzzy methods have evolved. Fuzzy filters, on the other hand, may preserve edges while also smoothing up the image, unlike most classical filters. Fuzzy filters may convey information in a more understandable manner than other nonlinear methods. In this study, we show and compare the outcomes of many distinct filtering methods.

Qiyuan Liang (2022) The cutting-edge performance of deep picture denoisers comes at a price. Recent research has shown that deep networks may overfit their training distributions, leading to incorrect hallucinations and poor generalization to new data. We offer a new framework that takes use of a denoising network for enhanced control and interpretability of a deep denoiser. We refer to this process as "controllable confidence-based picture denoising" (CCID). In this setup, we take use of both the results of a deep denoising network and a convolved picture with a trustworthy filter. A basic convolution kernel poses no danger of introducing phantasmal data and may serve as such a filter. Using a frequency-domain method that accounts for the robustness of the deep network outputs, we suggest fusing the two halves together. We've designed a system where the user has direct control over the frequency-domain fusion of the two parts. In addition, we include a user-friendly map for calculating the likelihood that the network's output is contaminated by hallucinations. In particular, when test data deviate from training data, our CCID is shown to beat both the deep denoiser and the dependable filter quantitatively.

Kai Zhang (2017) Due to its superior denoising performance, discriminative model learning for image denoising has lately garnered a lot of interest. In this study, we make a first step toward incorporating the latest advancements in extremely deep architecture, learning algorithm, and regularization technique into picture denoising by exploring the building of feed-forward denoising convolutional neural networks (DnCNNs). The training process is accelerated, and the denoising performance is improved, by using residual learning and batch normalization. Our DnCNN model is capable of handling Gaussian denoising with unknown noise level, which sets it apart from current discriminative denoising models, which typically train a particular model for additive white Gaussian noise at a specified noise level (i.e., blind Gaussian denoising). DnCNN uses a residual learning

technique that automatically discards the concealed clean image. Based on this feature, we train a single DnCNN model to deal with a wide variety of general image denoising tasks, including Gaussian denoising, single image super-resolution, and JPEG image deblocking. Extensive studies show that our DnCNN model can not only be easily implemented with the help of GPU computing, but that it can also show great efficacy in numerous generic image denoising applications.

Majed El Helou (2020) Using a special model that can denoise photographs with any amount of noise is what is meant by "blind and universal image denoising." It's a great option for real-world use since it doesn't need knowing the degree of background noise either during model creation or testing. To get rid of additive Gaussian noise, we offer a blind and universal deep learning picture denoiser that is based on theory. The foundation of our network is fusion denoising, a state-of-the-art approach to denoising. It is theoretically developed using the Gaussian image prior hypothesis. Our network exhibits excellent generalization to additive noise levels that are not seen in synthetic trials. For denoising actual pictures, we additionally modify the fusion denoising network structure. The PSNR results of real-world grayscale additive picture denoising are improved by our method, both for noise levels encountered during training and for noise levels not seen during training. Additionally, it enhances the performance of state-of-the-art color picture denoising on all noise levels by an average of 0.1dB, regardless of whether the image was trained on or not.

3. METHODOLOGY

The filter presented in this study is a filter for pictures that combines the L2-norm and GF (hence referred to as L2GFI) (hereinafter referred to as L2GFI). What follows are bullet points outlining the algorithm behind the suggested approach. We also utilized MATLAB to create the suggested technique.

- The original image's coordinates are used to determine where to place the reference points in a grid of cells.
- A Gaussian distribution is imposed along the x and y axes;
- When the weight value does not go to zero in a row, the region of space in z-coordinate is called a weight mountain, and
- Maximum weight is used to choose which mountain to climb;
- The final result is determined by convolving the normalized weights with the z value of each pixel inside the specified mountain range.

Besides the x, y, and z coordinates, you can also supply a value for the pixel in an array. Therefore, in the case of two-dimensional grayscale pictures, processing the L2GFI calls for a three-dimensional array. Each pixel's x-coordinate, y-coordinate, and z-value are recorded in separate tables, and the L2GFI draws reference points in these tables. Each pixel's reference points are plotted, and the GF is applied to them in the xy plane. When it happens, the relevant cell gets an extra GF weight array. When calculating the L2GFI method, once the GF has been applied, the pixel-by-pixel weight distribution along the z axis is examined. We call that mountain of weight, that region where the weight value doesn't go to zero in a row. At that time, mountains that are close together in proximity are considered to be a single mountain. Only data from the part of the mountain where the total weight is greatest is used to get the final result. The final result is the product of the normalized weights and the z value of each pixel. The result of L2GFI may be stated as Equation (1), where z_1, z_2, \dots, z_n are the pixel values in the computation range, w_1, w_2, \dots, w_n are the weights of the Gaussian function, and o is the output value.

$$o = \sum_{i=1}^n z_i w_i$$

In Figure 2, we can see a comparison between the two cases, where the target pixel is either a normal value or noise. when the target pixel has a normal value, the surrounding pixels also have normal values. When the target pixel is noisy (as illustrated in Figure 2), the nearby pixels are also visible. Weight distribution along the z-axis, GF output process, and L2GFI output process after being applied using GF. depicts the results of applying the GF, including the resulting z-axis weight distribution, the GF's output process, and the L2GFI's output process. When comparing the GF output values in, it can be seen that the GF output value in deviates from the normal value more than the GF output value.

Since the GF conducts computations along the complete z-axis, its output value is subject to noise. the L2GFI's output values side by side, indicating that they are identical. This is because the L2GFI prioritizes information from the mountain range with the highest overall weight when calculating its output values. This is why top-notch denoising performance is a target for L2GFI. When L2GFI (of size 5 5) is applied to an area that contains borders, , the weight distribution reveals two mountains. The mountains that include the target pixel have a larger aggregate weight due to a property of the Gaussian function. Because the L2GFI only uses the pixel values of the edge that includes the target pixel to calculate its output value, it is able to preserve the edges. Moreover, even when noise is present in the edges, the L2GFI is able to eradicate the noise without blurring the edges, The L2GFI is expected to have strong edge-preserving capabilities since the same processing may be applied to more pixels.

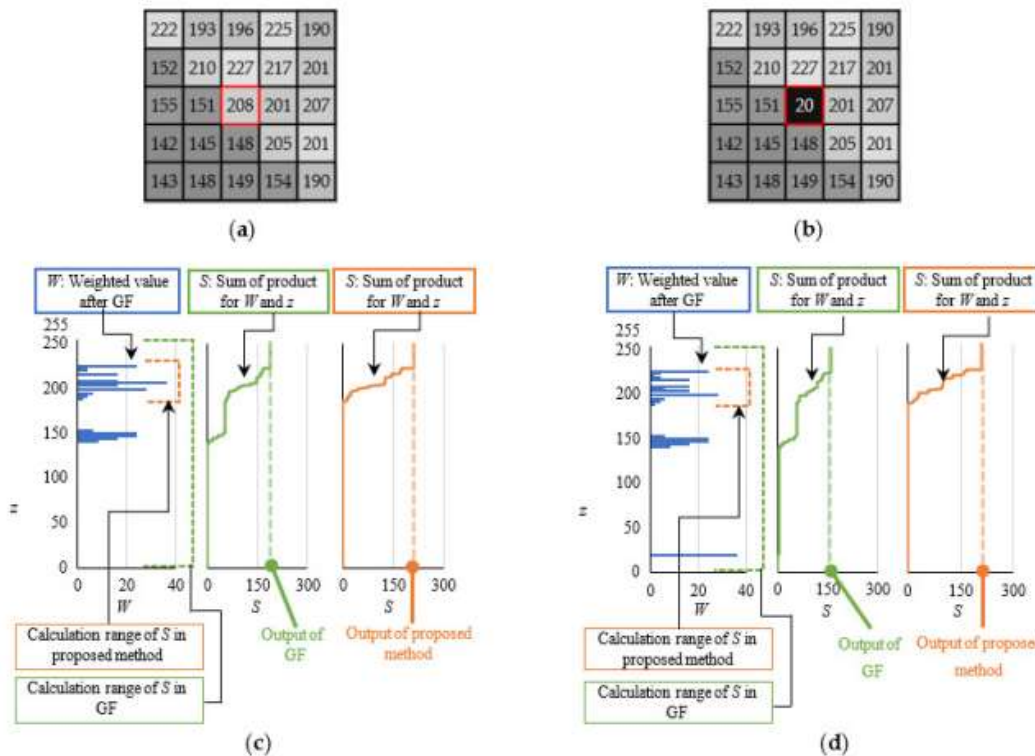


Figure 2. Comparison of output processing of normal value and noise when using GF and L2GFI; (a) sample image of only normal values; (b) sample image with noise; (c) output processing of GF and L2GFI for (a); (d) output processing of GF and L2GFI for (b).

Noise Reduction Experiment

The results of the L2GFI algorithm's denoising and edge-preserving capabilities are validated here. The L2GFI and NLMF are both applied to a sample picture with noise introduced, and their denoising and edge-preserving abilities are compared using root-mean-square error and human assessment (RMSE). It may be claimed that the reproducibility of the original picture improves as the RMSE value decreases. A better replication of the source picture suggests stronger denoising and edge-preservation skills. Three kinds of standard photographs are utilized as sample photos for the experiment.

The example picture has a resolution of 256 pixels by 256 pixels. Each filter is applied with a size of 5 pixels by 5 pixels. In this test, the NLMF is utilized as an OpenCV 4.5.3 function to prevent implementation issues. Parameters of the NLMF are set according to the optimal values for the corresponding function. Figures 3–5 show the original picture, noise-added image, and outcome of applying each filter on the noise-added image for each sample image. Figures 3–5 show the results of each filter, which are contrasted visually. When comparing the NLMF's output picture to the image with noise introduced, no significant differences were found in any of the samples. It can be proven that the NLMF has a good edge-preserving performance, and a low denoising performance for strong noise. In every case, noise removal was visible in the L2GFI's output picture. Therefore, it can be shown that the L2GFI has greater denoising and edge-preservation capabilities compared to the NLMF.

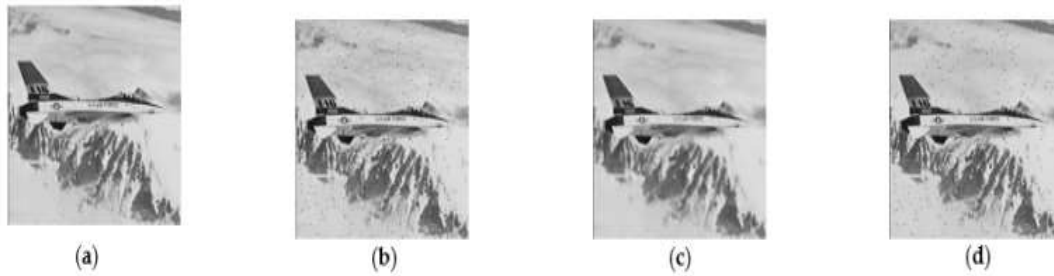


Figure 3. Filtering results for sample image “Airplane“; (a) input image; (b) image with noise added to (a); (c) filtering result of (b) by L2GFI; (d) filtering result of (b) by NLMF

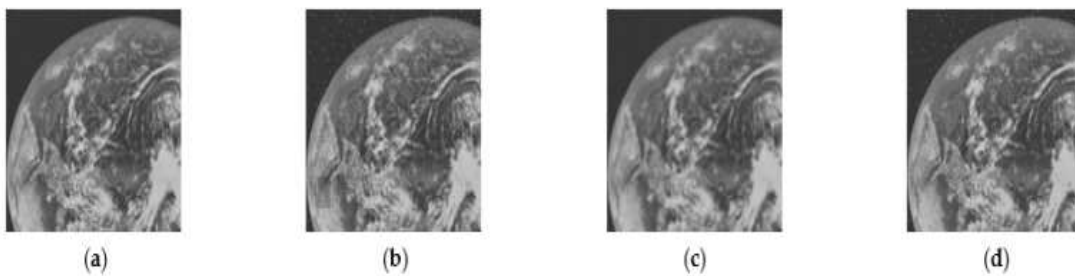


Figure 4. Filtering results for sample image “Earth“; (a) input image; (b) image with noise added to (a); (c) filtering result of (b) by L2GFI; (d) filtering result of (b) by NLMF.



Figure 5. Filtering results for sample image “Girl“; (a) input image; (b) image with noise added to (a); (c) filtering result of (b) by L2GFI; (d) filtering result of (b) by NLMF.

In Table 1, we see the RMSE values for each filter (first row) and the deviation ratio (percentage) from the RMSE values for the L2GFI (second row) for each example picture. Table 1's first row demonstrates that NLMF's RMSE is greater than L2GFI's. Table 1's second row displays the magnitude of the difference between the RMSE values for NLMF and L2GFI. All of the example pictures in Table 1 have RMSE values for the L2GFI that are 34% or lower than those for the NLMF. Based on the RMSE values, the L2GFI may be claimed to have superior denoising and edge-preservation capabilities compared to the NLMF.

Table 1. RMSE values calculated using each filter (upper section) and deviation ratio (%) from RMSE value calculated using L2GFI (lower section)

Sample Image	L2GFI	NLMF
Airplane	9.47	14.55
	-	34.88
Earth	5.94	13.56
	-	56.23
Girl	5.20	15.04
	-	65.38

Computer Time Validation of L2GFI's fast processing speeds. L2GFI and NLMF processing times are compared in this experiment. To gauge the software's efficiency, we relied on its built-in tools for timing the various stages of processing. For the purpose of this comparative experiment, we applied the filter 10 times and took the mean processing time. This experiment replicates Section 3.1's experiment with the identical sample photos and filter parameter settings. As can be seen from the experiment, the L2GFI has an average processing time of 0.2 s, whereas the NLMF has an average processing time of 17.6 s. When compared to the NLMF, L2GFI's processing time is 88 times quicker. We determined the standard deviation of the data for 10 separate measurements to confirm the precision of the measurement. Assuming a coverage factor of 2, the L2GFI takes 0.2 ± 0.014 s to calculate, with a standard deviation of 0.007 (s). Therefore, the NLMF's computation time is 17.6 ± 0.02 s ($k = 2$), where s is the standard deviation of the calculation time. In this case, the measurements have a low margin of error. The L2GFI also outperforms the NLMF when it comes to high-speed processing.

4. CONCLUSION

It has been suggested that the soft morphological filter be used for the purpose of reducing periodic noise. When compared with alternative spatial domain approaches, such as the classic morphology filter, it achieves the desired performance. When compared to traditional frequency domain approaches, the soft morphology filter is both simpler to construct and more efficient computationally. In this study, we combined the GF with the L2-norm to present the L2GFI, a noise reduction filter for pictures that can maintain edge quality. Here are the findings from that study. First, the L2GFI outperformed the NLMF in terms of denoising and edge-preservation in an eye-to-eye comparison of experimental findings. The RMSE values for L2GFI were at least 34% less than those for the NLMF, as shown by experiments. As a result, we can state that the L2GFI's original picture is more reproducible than the NLMF's. Third, the L2GFI had a shorter processing time than the NLMF, according to the verification findings. So, when it comes to high-speed processing, L2GFI is preferable than NLMF. It can be concluded from these findings that the L2GFI, in comparison to the NLMF, combines superior denoising, edge-preservation, and processing speed. We reasoned that more validation of the L2GFI's performance is necessary before it could be used in the real world. So, we will test the L2GFI's efficacy with more complicated sample pictures and more kinds of noise in the future.

5. REFERENCES

1. Dumitrescu, Catalin. (2020). EVALUATE THE QUALITY OF PROCESSED IMAGES IN TERMS OF NOISE REDUCTION AND CONTOUR PRESERVATION. *Engineering Sciences*. 12. 22-32.
2. Hambal, Abdalla Mohamed and Zhijun Pei. "Image Noise Reduction and Filtering Techniques." (2017).
3. Qiyuan Liang (2022) "Image Denoising with Control over Deep Network Hallucination" arXiv:2201.00429v1 [eess.IV] 2 Jan 2022
4. Kai Zhang, Wangmeng Zuo, Yunjin Chen, Deyu Meng, and Lei Zhang. Beyond a Gaussian denoiser: Residual learning of deep CNN for image denoising. *IEEE Transactions on Image Processing*, 26(7):3142–3155, 2017
5. Majed El Helou and Sabine Susstrunk. Blind universal Bayesian " image denoising with Gaussian noise level learning. *IEEE Transactions on Image Processing*, 29:4885–4897, 2020.
6. Khaung Tin, Dr.Hlaing Htake. (2011). Removal of Noise Reduction for Image Processing.
7. Shuhang Gu, Lei Zhang, Wangmeng Zuo, and Xiangchu Feng. Weighted nuclear norm minimization with application to image denoising. In *Proceedings of the IEEE/CVF Conference on Computer Vision and Pattern Recognition (CVPR)*, pages 2862–2869, 2014.
8. Chang Chen, Zhiwei Xiong, Xinmei Tian, and Feng Wu. Deep boosting for image denoising. In *Proceedings of the European Conference on Computer Vision (ECCV)*, pages 3–19, 2018.

9. W. Dong, L. Zhang, and G. Shi, "Centralized sparse representation for image restoration," in Proc. Int. Conf. Comput. Vis., Nov. 2011, pp. 1259–1266.
10. W. Dong, L. Zhang, G. Shi, and X. Li, "Nonlocally centralized sparse representation for image restoration," IEEE Trans. Image Process., vol. 22, no. 4, pp. 1620–1630, Apr. 2013
11. S. Gu, L. Zhang, W. Zuo, and X. Feng, "Weighted nuclear norm minimization with application to image denoising," in Proc. IEEE Conf. Comput. Vis. Pattern Recognit., Jun. 2014, pp. 2862–2869.
12. M. Hasan and M. R. El-Sakka, "Improved BM3D image denoising using SSIM-optimized Wiener filter," EURASIP J. Image Video Process., vol. 2018, no. 1, p. 25, Apr. 2018.
13. Y. Le Montagner, E. D. Angelini, and J.-C. Olivo-Marin, "An unbiased risk estimator for image denoising in the presence of mixed Poisson–Gaussian noise," IEEE Trans. Image Process., vol. 23, no. 3, pp. 1255–1268, Mar. 2014
14. S. Lefkimmiatis, "Non-local color image denoising with convolutional neural networks," in Proc. IEEE Conf. Comput. Vis. Pattern Recognit. (CVPR), Jul. 2017, pp. 3587–3596.
15. D. Liu, B. Wen, X. Liu, Z. Wang, and T. Huang, "When image denoising meets high-level vision tasks: A deep learning approach," in Proc. 27th Int. Joint Conf. Artif. Intell., Jul. 2018, pp. 842–848.

